



Research articles

Perpendicular magnetic anisotropy and residual magnetic phases in gold-capped FeRh film on MgO(0 0 1)



P. Drózdź^{a,*}, M. Ślęzak^a, K. Matlak^a, K. Freindl^b, N. Spiridis^b, D. Wilgocka-Ślęzak^b,
A. Koziół-Rachwał^a, J. Korecki^{a,b}, T. Ślęzak^a

^a AGH University of Science and Technology, Faculty of Physics and Applied Computer Science, Aleja Adama Mickiewicza 30, 30-059 Kraków, Poland

^b Jerzy Haber Institute of Catalysis and Surface Chemistry, Polish Academy of Sciences, 30-239 Kraków, Poland

ARTICLE INFO

Keywords:

Magnetism
Phase transition
Magnetic anisotropy
FeRh alloy
Thin films
Epitaxy

ABSTRACT

We studied the magnetic properties of 10 and 20 nm-thick, gold-capped FeRh layers grown on MgO(001). Whereas the majority of the FeRh film undergoes ferromagnetic–antiferromagnetic phase transition upon cooling, a small fraction of the FeRh system remains in the ferromagnetic state at low temperatures. This residual ferromagnetic phase located at the FeRh/MgO interface exhibits perpendicular magnetic anisotropy. Moreover, in the 10 nm-thick film, a small amount of the antiferromagnetic phase survives to high temperatures above the phase transition and probably originates from the epitaxial strains generated at the FeRh/Au interface.

1. Introduction

The FeRh alloy with equiatomic composition undergoes a first-order temperature magnetic phase transition from an antiferromagnetic (AFM) to ferromagnetic (FM) state at a transition temperature close to 350 K [1–3]. Recently, low-dimensional FeRh films showing AFM–FM transition have attracted much attention as important materials for new storage media applications, such as heat-assisted magnetic recording [4,5], AFM memory resistor [6], magnetic refrigerators [7] and picosecond regime switching of FM order [8]. In the case of MgO-supported FeRh films, several experiments reported the presence of a residual FM phase in a nominally AFM system. For the uncoated FeRh/MgO system, a FM surface state was observed to coexist with the AFM volume [9], in contrast to the MgO/FeRh/MgO system, where the residual FM phase was found at the FeRh/MgO interface [10]. The existence of a FM fraction with out-of-plane magnetic anisotropy coexisting with the AFM phase was theoretically predicted by Odkhuu [11,12]. The magnetic anisotropy of FeRh films is strongly dependent on the elastic strains induced at the interfaces that can generate both in- and out-of-plane magnetic anisotropy [13–15]. The surface termination of FeRh influences the nature of magnetic anisotropy and its strength as previously shown theoretically [16–18]. Finally, recent ab initio calculations [19] indicate that the tetragonal distortion has a strong impact on the FeRh magnetic order, leading to the possible coexistence of different AFM phases.

In this report, we show that the FM–AFM phase transition on

cooling is not complete in 10 and 20 nm-thick FeRh layers grown on MgO(0 0 1) and capped by an epitaxial 3 nm gold layer. In addition, the remaining residual FM phase located at the FeRh/MgO interface exhibits perpendicular magnetic anisotropy (PMA). Moreover, in the case of the 10 nm-thick FeRh layer, the low-temperature mixed FM/AFM state does not transform to the homogenous FM state on heating, but instead, a fraction of the AFM phase persists at high temperatures and undergoes a direct phase transition to the paramagnetic state. Our results show that the presence of interfaces has a strong impact on the magnetic structure of a nominally simple system, resulting in its magnetic inhomogeneity at all temperatures. Moreover, the direction of the spontaneous magnetization of the FM phase can be temperature controlled by the AFM–FM phase transition between out-of-plane and in-plane directions.

2. Experimental details and structural studies

The 10 and 20 nm-thick FeRh layers were grown on polished MgO(0 0 1) single crystals by elemental co-deposition at 670 K. The ⁵⁷Fe was evaporated from a resistively heated BeO crucible, while the evaporation of Rh was realized by electron bombardment. The nominal Rh atomic concentration established by adjustment of the Fe and Rh evaporation rates (both in a range of Å/min) was approximately 54%. The samples were post-annealed at 1000 K for 1 h to promote the formation of the desired B2 structure [20] and capped by a 3 nm-thick epitaxial Au(0 0 1) film. The epitaxial character of the FeRh film was shown by

* Corresponding author.

E-mail address: piotr.drozd@fis.agh.edu.pl (P. Drózdź).

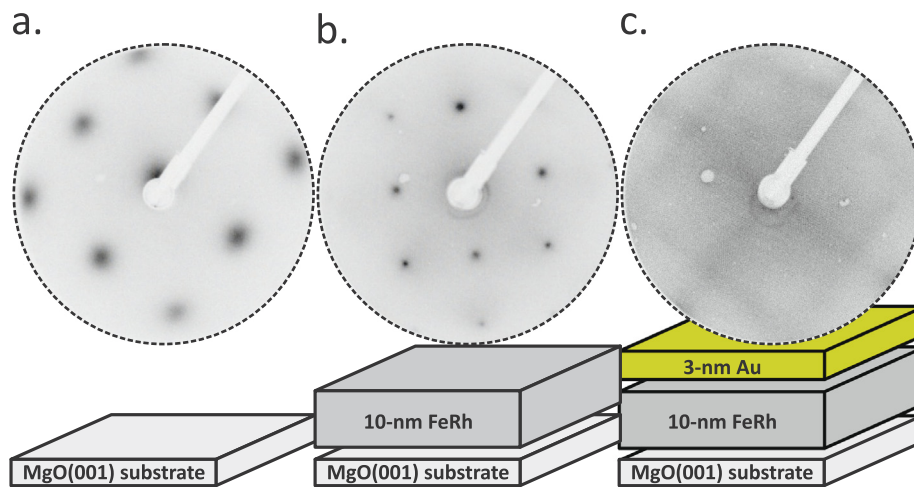


Fig. 1. The LEED patterns collected with an electron beam energy of 70 eV for: (a) MgO(0 0 1) substrate, (b) 10 nm-thick FeRh and (c) 3 nm-thick gold-capped layer.

low-energy electron diffraction (LEED) patterns (Fig. 1), in which a LEED pattern for the 10 nm-thick FeRh film was compared with these of the MgO(0 0 1) substrate and Au overlayer. The FeRh pattern is characterized by sharp diffraction spots and low background, indicating the high structural quality of the FeRh system. Comparison of the LEED patterns of the MgO(0 0 1) substrate and FeRh alloy indicates a 45° in-plane rotation of the MgO(0 0 1) and B2 FeRh(0 0 1) surface unit cells. Similar rotational relations were found between the fcc Au(0 0 1) and FeRh(0 0 1) surfaces. The diffraction pattern of the Au(0 0 1) surface is weak, although traces of a typical Au(0 0 1) (5 × 1) reconstruction can be seen [21]. The structural characterization was supported by X-ray diffraction measurements in θ -2 θ scattering geometry. The X-ray diffraction pattern (not shown) clearly indicated the formation of the B2 FeRh phase manifested by the presence of (0 0 1), (0 0 2) and (0 0 3) reflections, and the absence of peaks corresponding to the chemically disordered fcc γ -phase of the FeRh, similarly to Inoue et al. [22].

3. Results and discussion

The magnetic properties were studied with polar (PMOKE) and longitudinal magneto-optic Kerr effect (LMOKE) geometries in a temperature range between 80 K and 360 K. To obtain the temperature dependence of the FeRh magnetization, the magnetic hysteresis loops were collected during a cooling \Leftrightarrow heating cycle and the value of Kerr rotation at saturation (normalized to the value at 359 K) was taken as a measure of the FeRh magnetization similarly to previous procedures [23,24]. The exemplary PMOKE and LMOKE hysteresis loops measured for the 10 nm-thick FeRh at 80 K and 340 K are shown in Fig. 2a and b, respectively. The typical hard-axis PMOKE loop compared with almost-rectangular LMOKE loops indicates an in-plane magnetic anisotropy of the FeRh system at 340 K (see Fig. 2b). At 80 K (Fig. 2a), the character of the PMOKE and LMOKE hysteresis curves interchanges, i.e., the LMOKE loop is hard-axis-like, while the PMOKE loop is characterized by significant values of the remanence Kerr signal and hysteresis, which indicates the existence of a FM phase with perpendicular magnetization. The MOKE data were systematically collected during the temperature cycle 350 K \Rightarrow 80 K \Rightarrow 350 K. The evolution of the PMOKE and LMOKE loops on cooling is shown in the top and bottom plots of Fig. 2c, respectively. With decreasing temperature, the saturation of the Kerr signal decreases, but the PMOKE loops simultaneously change their shapes from typical hard-axis loops to a loop with large remanence Kerr signal and non-zero coercivity.

In Fig. 3a, a temperature dependence of the PMOKE Kerr rotation at saturation and remanence normalized to the saturation value for each loop (denoted as ROT_{SAT} and ROT_{REM} , respectively) are plotted as a function of temperature. $ROT_{SAT}(T)$, normalized to a saturation value at

359 K, reveals the presence of the FM \Leftrightarrow AFM transition characterized by typical thermal hysteresis. The transition extends over a wide temperature range and shifts towards low temperatures compared with the bulk, which is a typical behaviour for thin FeRh films on MgO [25]. Interestingly, along with the FM–AFM transition manifested by a gradual decrease of the ROT_{SAT} signal with decreasing temperature, a progressive increase in the PMOKE remanence signal can be observed. The $ROT_{REM}(T)$ dependence also displays thermal hysteresis and a negative correlation with the FM FeRh phase amount, here quantified by the ROT_{SAT} . An out-of-plane magnetization component proportional to the normalized ROT_{REM} signal clearly emerges at low temperatures. The straightforward interpretation of the above results can be based on the AFM–FM transition-controlled shape anisotropy of the FeRh system in combination with existence of a residual FM phase with PMA persisting down to low temperatures and coexisting with the AFM phase. This observation is in agreement with a recent theoretical calculation predicting the existence of an out-of-plane magnetized ultrathin FM layer at the MgO/FeRh interface [12]. The amount of the low-temperature FM phase can be estimated from the $ROT_{SAT}(T)$ curve (Fig. 3a) to be about 10% of the FM phase at high temperatures. The PMOKE hysteresis curve collected at 80 K (upper plot in Fig. 2a) is not rectangular, indicating a not fully out-of-plane magnetization state that can be realized by a vertical non-collinearity of magnetic structures or the formation of magnetic domains. An estimation of the average perpendicular magnetization component based on the normalized ROT_{REM} gives approximately half of the saturation value, which roughly corresponds to a range of 1–2 FeRh monolayers of spontaneous perpendicular magnetization. With increasing temperature, the AFM–FM transition takes place and the overall magnetic anisotropy becomes dominated by the shape anisotropy that gradually increases as the FM phase develops. Fig. 3a shows that both on heating and cooling, roughly in the middle of the transition, the magnetic anisotropy is already in-plane as indicated by a negligible normalized ROT_{REM} signal. PMA is observed when the amount of FM phase drops below 50%.

Similar MOKE studies were performed for the analogous 20 nm-thick FeRh system. The LMOKE data indicated that the profile of the AFM–FM transition is shifted towards higher temperatures (by approximately 140 K) in comparison to the 10 nm-thick film (Fig. 3b). In parallel, no out-of-plane magnetization component was observed with PMOKE in the whole investigated temperature range.

To get deeper insight into the spin structure of our MgO/FeRh/Au samples and its temperature-driven evolution, conversion electron Mössbauer spectroscopy (CEMS) measurements were performed in a wide temperature range using an ultra-high vacuum CEMS setup with a 100-mCi $^{57}\text{Co}(\text{Rh})$ source in normal incidence geometry and channeltron detection. The measured spectra were analysed using commercial

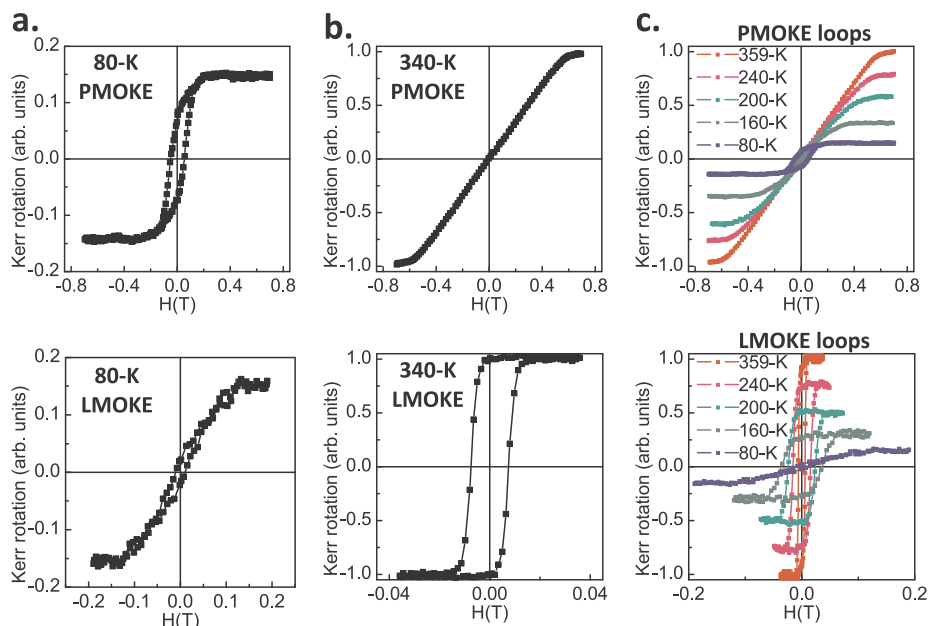


Fig. 2. Exemplary magnetic hysteresis loops collected for PMOKE (top plots) and LMOKE geometry (bottom plots) for (a) 80 K and (b) 340 K. (c) Temperature evolution of the magnetic loops collected on cooling for both MOKE geometries.

software and the fitting procedure was based on the hyperfine magnetic field distribution (HFD) represented by a sum of Gaussian components [26].

In Fig. 4a–d, the CEMS spectra for the 10 nm sample are shown for the selected temperatures on the heating branch. A satisfactory fit of the spectrum collected at 112 K (nominally corresponding to the AFM FeRh state) could be obtained, assuming seven components (see Fig. 4a). The vertical bars on the right side of each spectrum present relative contribution of the selected components. The dominant blue component (total contribution 82%) with a bi-modal distribution of the HFD with maxima of HFD at $B_{HF1} = 26.6$ T and $B_{HF2} = 24.1$ T is attributed to the AFM phase. The two Gaussian sub-components of the AFM phase are interpreted in the following way: i.e., the sharp component with $B_{HF1} = 26.6$ T and a fraction $f_{AFM1} = 62\%$ of the total spectral area corresponds to the Fe sites in the ideal CsCl structure with all Rh nearest neighbours (nn) and all Fe next nearest neighbours (nnn). The broader sub-spectrum with $B_{HF2} = 24.1$ T and $f_{AFM2} = 20\%$ is connected to the Fe atoms with Rh atoms substituting some of Fe nnn due to excess of Rh caused by the deviation from the perfect equi-atomic stoichiometry of our FeRh alloy (54% of Rh in our case). The amount of such defected Fe

sites can be estimated from the contribution of the AFM₂ component to be about 3% of all Fe sites because the single antistructure Rh atom disturbs eight neighbouring Fe sites. The intensity ratio of the second and third lines of the Mössbauer sextet, $R_{2/3}$, which is a fingerprint of the hyperfine field orientation for the AFM component 4:1, indicates (for the normal incidence geometry) an in-plane direction of the hyperfine magnetic field and hence in-plane magnetic anisotropy of the AFM FeRh phase.

The second component (red hatched area in Fig. 4a) with $B_{HF3} = 30.3$ T and contribution $f_{FM1} = 3.5\%$ is attributed to a residual low-temperature FM phase. In this case, the $R_{2/3}$ ratio is close to zero, which indicates the out-of-plane direction of B_{HF} and PMA of the residual FM phase. CEMS alone cannot always distinguish between the AFM and FM orders, but, in combination with the MOKE results, this is the only spectral component with an out-of-plane hyperfine field that can be associated with the low-temperature FM phase. According to the literature, the hyperfine magnetic field of the FM component should be higher by about 1.5–2 T with respect to the AFM component at given temperatures [27–29]. In the discussed spectrum, the difference in the hyperfine fields of the FM and AFM components is larger, which can be

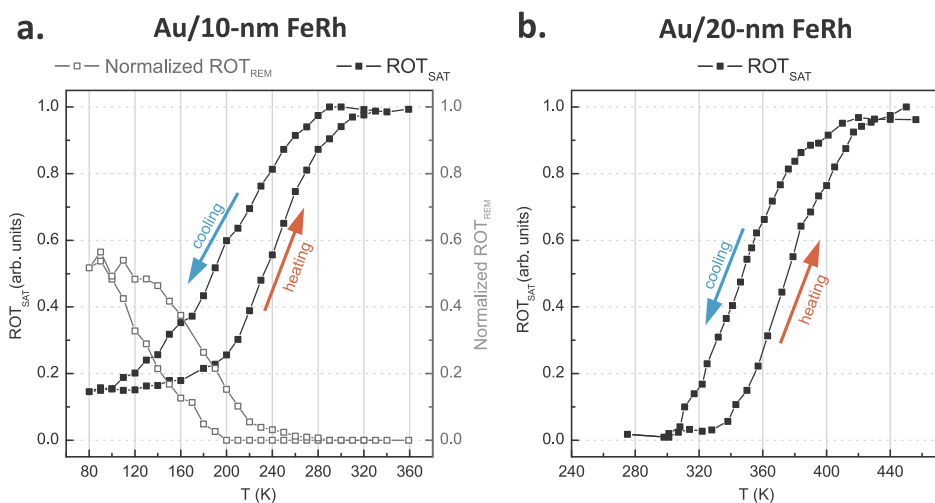


Fig. 3. (a) The temperature dependence of ROT_{SAT} (black filled squares) and normalized ROT_{REM} (open grey squares) for 10 nm-thick FeRh. (b) The temperature profile of the AFM-FM transition for 20 nm-thick FeRh. Blue and red arrows show the cooling and heating branches, respectively. (For interpretation of the references to colour in this figure legend, the reader is referred to the web version of this article.)

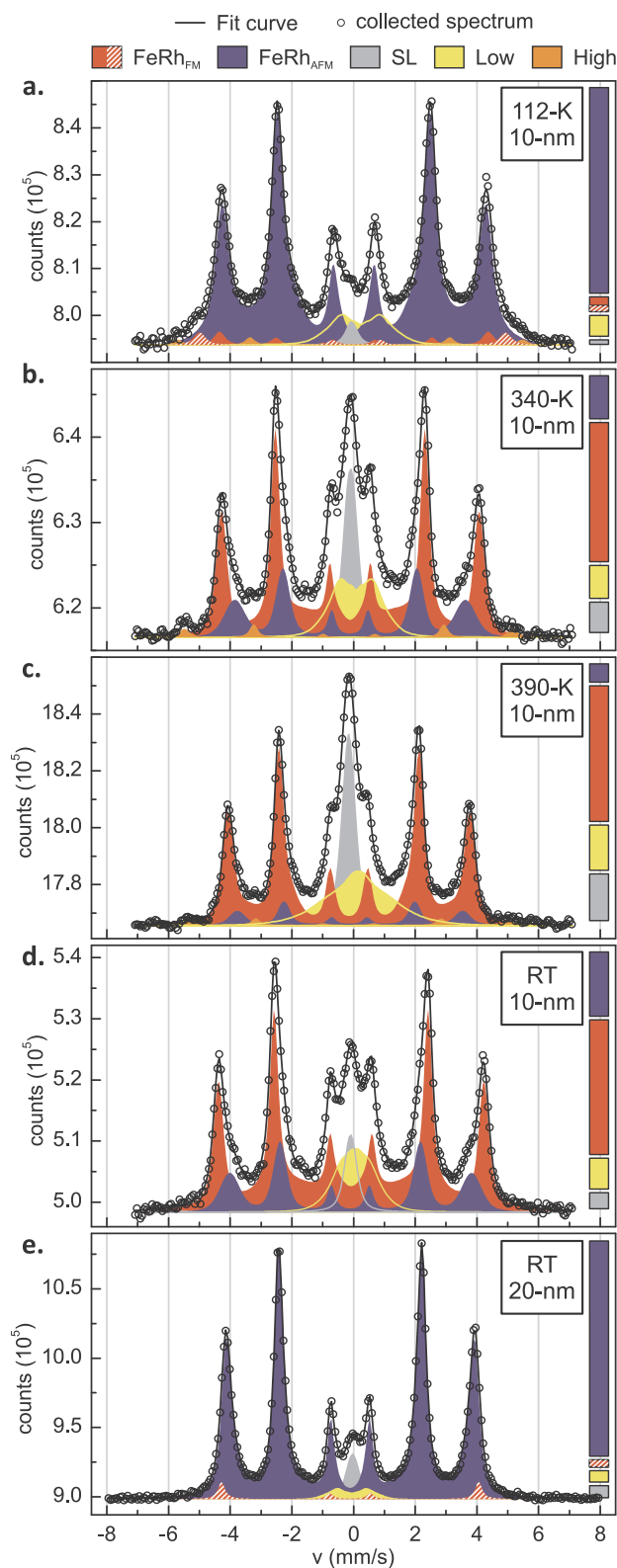


























Fig. 4. The CEMS spectra collected for Au/10 nm-thick FeRh/MgO(0 0 1) at (a) 112 K, (b) 340 K, (c) 390 K and (d) room temperature (RT). (e) The measured spectrum for Au/20 nm-thick FeRh/MgO(0 0 1) at RT. The vertical bars on the right side of each spectra present relative contribution of FM, AFM, SL and low field components. (For interpretation of the references to colour in this figure legend, the reader is referred to the web version of this article.)

explained by the proximity of the MgO substrate by analogy to a similar increase of B_{HF} reported at the Fe/MgO interface of epitaxial Fe(001) films [30]. In addition, a small fraction (~2.5%) of spectral area (shaded red) with canted orientation of B_{HF} ($B_{\text{HF}4} = 27.1$ T and $R_{2/3} = 1.5$) is also interpreted as corresponding to the ferromagnetic phase, being labelled by its isomeric shift higher by 0.02 mm/s with respect to sub-spectra corresponding to AFM phase. Such difference of isomer shifts of FM and AFM distinguishes the two magnetic phases as it is typically found for B2 ordered FeRh alloy [27,28]. The remaining three components are: i) a single line (shaded grey) with a fraction $f_{\text{SL}} = 2\%$ arising from a small contribution of a paramagnetic fcc γ -FeRh phase; ii) a low hyperfine magnetic field component ($B_{\text{LOW}} = 6$ T, $f_{\text{LOW}} = 8\%$, shaded yellow) corresponding to Fe atoms diffused into the Au cap in the vicinity of the FeRh/Au interface; and iii) a high-field component with $B_{\text{HIGH}} = 34$ T and a fraction $f_{\text{HIGH}} = 2\%$ (shaded orange) that is attributed to a small number of Fe antistructure atoms [27–29]. At such sites, all nn of a given Fe atom are also Fe atoms giving rise to Fe-metal-like magnetic hyperfine field values. B_{HIGH} is oriented in plane ($R_{2/3} = 4$), but it is difficult to judge whether FM or AFM states contribute to this component. Antistructure atoms are assumed to be randomly distributed in the volume of the FeRh film. The analysis of the 112 K CEMS spectrum coincides well with the MOKE data discussed above, which shows the existence of a residual FM phase with PMA. The CEMS data have shed some light on the location of the FM phase and revealed an in-plane direction of spins in the AFM phase.

Next, we discuss the CEMS spectrum collected at 340 K that corresponded to the FM state of our FeRh system according to our MOKE data (see Fig. 4b). The spectrum was fitted with a set of expected components considering the AFM–FM transition. The dominant spectral component with an in-plane hyperfine magnetic field spectral (shaded red, contribution of area of 55% and $R_{2/3} = 4$) corresponds to the FM phase. Its hyperfine magnetic field $B_{\text{HF}} = 25.7$ T in agreement with the literature [27,28] and its contribution relative to 112 K increased roughly by a factor of 10. This remains in good agreement with the MOKE measurements that are sensitive only to the FM FeRh phase. The low-temperature residual saturation Kerr rotation signal ROT_{SAT} is approximately 10 times smaller than the ROT_{SAT} at 340 K. All other components that were necessary to fit the low-temperature CEMS spectrum are also present. In particular, the high-field component has a similar contribution and a slightly lower magnetic hyperfine field, whereas the fractions of single-line and low-field components increased to about 12% and 14%, respectively. An unexpected feature of the 340 K CEMS spectrum is the significant contribution (17%) of the AFM component, which was unambiguously identified by $B_{\text{HF}} = 23.2$ T and isomer shift by 0.02 mm/s more negative than the FM component [27,28].

According to our MOKE results at 340 K, the AFM–FM transition was completed and no further increase of the FM FeRh phase was expected. Indeed, the CEMS spectrum measured at 390 K (see Fig. 4c) confirms that a fraction of the FM phase does not change. Instead, a further increase of the single-line contribution and simultaneous decrease of the AFM spectral component can be seen, which indicates that the AFM phase undergoes a transition not to FM, but to a paramagnetic phase. A noticeable increase of the low-field component (yellow sub-spectra in Fig. 4b–d) in comparison with the 112 K spectrum can be attributed to the transient state of the AFM phase between a stable magnetic order and a paramagnetic state. In the vicinity of the Néel temperature, a broadening of HFD and a lowering of B_{HF} is expected due to spin fluctuations. The transition of the AFM phase to the paramagnetic state is reversible, as confirmed by the analysis of a room temperature (RT) CEMS spectrum (see Fig. 4d) acquired after heating to 390 K, which again corresponds to saturated amount of FM phase as concluded from Fig. 3a. The area of FM spectral component (54%) is clearly very similar to the spectrum collected at 390 K. However, an increase of the AFM phase contribution (blue component with $B_{\text{HF}} = 24.6$ T) is accompanied by the decrease of the single-line and

Table 1
The hyperfine parameters derived from the numerical fits of CEMS spectra.

T	Component	IS* (mm/s)	H_{BF} (T)			Fraction (%)	$R_{2/3}$
112 K 10-nm	 FeRh _{AFM}	0.11(3)	26.6(1)	24.1(4)	82.0	4.0(1)	
	 FeRh _{FM}	0.12(5)	30.3(4)		3.5	0.0(5)	
	 FeRh _{FM}	0.13(5)	27.1(8)		2.5	1.5(8)	
	 Low	0.33(4)	6.0(5)		8.1	4.0(8)	
	 High	0.09(1)	34.0(6)		1.9	4.0(10)	
	 SL	0.03(4)	—		2.0	—	
340 K 10-nm	 FeRh _{AFM}	-0.02(1)	23.2(5)		17.0	3.9(5)	
	 FeRh _{FM}	0.00(1)	25.7(1)	15.8(4)	55.0	4.0(2)	
	 Low	0.19(6)	5.1(6)		14.0	4.0(8)	
	 High	-0.03(7)	33.0(6)		2.0	4.0(18)	
	 SL	0.00(3)	—		12.0	—	
390 K 10-nm	 FeRh _{AFM}	-0.05(5)	22.7(3)		7.3	4.0(6)	
	 FeRh _{FM}	-0.03(1)	24.4(1)	20.7(3)	54.0	4.0(1)	
	 Low	0.25(6)	6.6(2)		18.4	4.0(8)	
	 High	-0.06(7)	32.2(6)		1.7	4.0(22)	
	 SL	-0.06(1)	—		18.6	—	
RT 10-nm	 FeRh _{AFM}	0.00(2)	24.6(8)		26.7	4.0(3)	
	 FeRh _{FM}	0.02(1)	26.7(1)	18.5(2)	54.3	3.9(2)	
	 Low	0.16(3)	3.9(6)		12.4	3.8(20)	
	 SL	0.02(3)	—		6.6	—	
RT 20-nm	 FeRh _{AFM}	-0.01(1)	24.9(1)	24.2(2)	19.0(9)	88.1	4.0(1)
	 FeRh _{FM}	0.01(5)	25.8(2)		3.2	0.0(1)	
	 Low	0.05(4)	4.7(2)		3.4	4.0(9)	
	 SL	0.07(1)	—		5.3	—	

*IS is the average isomer shift with respect to α -Fe.

low-field component areas that correspond to the paramagnetic and transient states, respectively. Our results show that in the temperature range nominally corresponding to the FM state (above 320 K), a significant fraction of the AFM phase reversibly undergoes transition to the paramagnetic state. Moreover, a significant increase of magnetic hyperfine field can be noticed on cooling from 390 K to RT. We suppose that such behaviour is closely connected to the temperature dependence of magnetization in analogy with interpretation of B_{HF} (T) proposed by Shirane for bulk FeRh [28]. To ensure the clarity of above discussion the hyperfine parameters derived from the numerical fits of CEMS spectra are listed in Table 1.

The spin structure of the MgO/10 nm-thick FeRh/Au system derived from the combined CEMS/MOKE data analysis at low and high temperatures is schematically shown in Fig. 5. At low temperature, the interfacial FM phase with PMA coexists with bulk-like AF phase with in-plane spin orientation (left panel in Fig. 5). At high temperatures corresponding to the nominally FM state of FeRh, both FM and AFM phases still coexist with in-plane magnetic anisotropy (right panel in Fig. 5).

Additional support for our interpretation comes from the analysis of magnetic properties of the MgO/20 nm-thick FeRh/Au system for which the RT CEMS spectrum is shown in Fig. 4e. At RT, the 20 nm-thick film is in the AFM state, as can be seen from the temperature profile of the AFM–FM transition shown in Fig. 3b. Indeed, the AFM (shaded blue) spectral component with average $B_{HF} = 24$ T and fraction $f_{AFM} = 88\%$ dominates the CEMS spectrum. However, a component characterized by $B_{HF} = 25.8$ T with a contribution $f_{FM} = 3\%$ and $R_{2/3}$ ratio equal to 0 is also present (red hatched area). The isomer shift difference of the two components (0.02 mm/s) indicates that the latter magnetic sub-spectrum with out-of-plane B_{HF} corresponds to a residual FM phase coexisting with the AFM phase, similar to the MgO/10 nm-thick FeRh/Au system. The lower (by a factor of 2) contribution of the residual FM phase confirms its interfacial nature. No perpendicular magnetization component was observed in PMOKE, which clearly points to the conclusion that the FM fraction with PMA resides at the vicinity of MgO/FeRh interface. For the MgO/20 nm-thick FeRh/Au system, the MgO/FeRh interface is deeply buried and invisible in MOKE measurements. Finally, the interpretation of the RT CEMS spectrum of

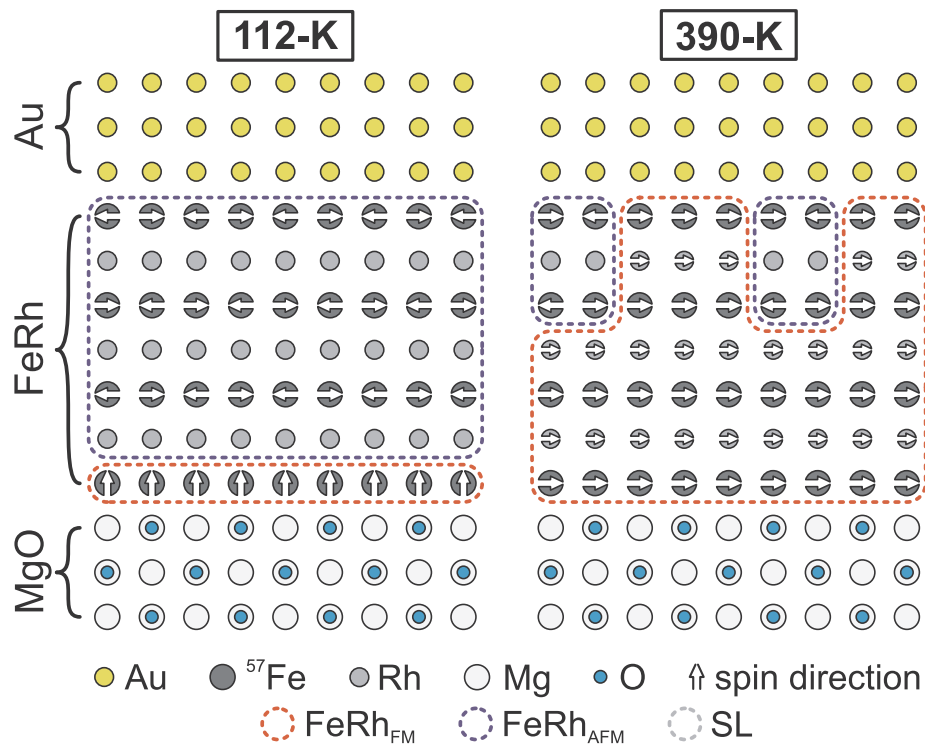


Fig. 5. A simplified schematic of the spin structure of the MgO/10 nm-thick FeRh/Au system derived from MOKE and CEMS studies at low and high temperatures. For clarity, only the FM and AFM phases are pictured and the paramagnetic- and defect-related sites are omitted.

MgO/20 nm-thick FeRh/Au sample agrees well with the analysis of the CEMS data of MgO/10 nm-thick FeRh/Au collected at RT after heating to 390 K. At RT, two spectral components with $B_{HF} = 24$ T and $B_{HF} = 25.8$ T represent the AFM and FM phases, respectively. However, the dominating AFM phase coexists at RT with a small amount of the FM phase (with PMA) in the case of MgO/20 nm-thick FeRh/Au, but the FM phase dominates in the MgO/10 nm-thick FeRh/Au system while a significant amount of the AFM fraction is simultaneously also present. The origin of the residual AFM phase in the nominally FM state of FeRh is not obvious; however, a compressive strain at the FeRh/Au interface arising from the large misfit between the in plane lattice parameters of FeRh(0 0 1) ($a_{FeRh} = 3$ Å) and fcc-Au(0 0 1) ($a_{Au} = 2.88$ Å) can be responsible for stabilization of the AFM phase that does not undergo the AFM–FM phase transition [19]. In parallel, a definite location or distribution of residual AFM phase cannot be obtained on the above-mentioned results. However, our experimental findings concerning FeRh/Au/Fe [24] and preliminary unpublished data for FeRh/Au/FeAu trilayers indicate that the indirect exchange coupling between FeRh and Fe (FeAu) sublayers that is mediated across the Au spacer strongly depends on the amount of FM FeRh phase. The existence of a thin and continuous film of the AF FeRh phase neighbouring the Au film would most probably suppress the interaction between the FM phase of FeRh and the top magnetic sublayer in the FeRh/Au/Fe and FeRh/Au/FeAu systems. Hence, the presence of continuous AF FeRh phase is not probable, but instead we suppose that it may nucleate in the form of discontinuous patches in the vicinity of the FeRh/Au interface (Fig. 5).

4. Conclusion

In conclusion, we showed that in gold-capped FeRh layers grown on MgO(0 0 1) phase transition from FM to AFM on cooling is incomplete, and the residual FM phase located at the FeRh/MgO interface exhibits PMA. Moreover, on heating, the low-temperature mixed FM/AFM state does not fully transform to the homogenous FM phase, but a fraction of the AFM phase survives to high temperatures.

Declaration of Competing Interest

There is no conflict of interest.

Acknowledgments

This work is supported by the National Science Center Poland under Project No. 2015/19/B/ST3/00543 and partially by the AGH University of Science and Technology statutory task No. 11.1.1.220.01/6 within subsidy of the Ministry of Science and Higher Education. N. Spiridis and D. Wilgocka-Ślęzak thank for support statutory research funds of ICSC PAS.

References

- [1] J.S. Kouvel, C.C. Hartelius, Anomalous magnetic moments and transformations in the ordered alloy FeRh, *J. Appl. Phys.* 33 (1962) 1343.
- [2] M. Fallot, Les Alliages Du Fer Avec Les Métaux de La Famille Du Platine, *Ann. Phys.* 10 (1938) 291.
- [3] M. Fallot, R. Hocart, Sur L'apparition Du Ferromagnétisme Par Élévation de Température Dans Des Alliages de Fer et de Rhodium, *Rev. Sci.* 77 (1939) 498.
- [4] J. Thiele, S. Maat, E.E. Fullerton, FeRh/FePt exchange spring films for thermally assisted magnetic recording media, *Appl. Phys. Lett.* 82 (2003) 2859.
- [5] M.H. Kryder, E.C. Gage, T.W. McDaniel, W.A. Challener, R.E. Rottmayer, G. Ju, Y.T. Hsia, M.F. Erden, Heat assisted magnetic recording, *Proc. IEEE* 96 (2008) 1810.
- [6] X. Marti, I. Fina, C. Frontera, J. Liu, P. Wadley, Q. He, R.J. Paull, J.D. Clarkson, J. Kudrnovský, I. Turek, J. Kuneš, D. Yi, J. Chu, C.T. Nelson, L. You, E. Arenholz, S. Salahuddin, J. Fontcuberta, T. Jungwirth, R. Ramesh, Room-temperature anti-ferromagnetic memory resistor, *Nat. Mater.* 13 (2014) 367.
- [7] E. Stern-Taulats, A. Planes, P. Lloveras, M. Barrio, J.L. Tamarit, S. Pramanick, S. Majumdar, C. Frontera, L. Mañosa, Barocaloric and magnetocaloric effects in Fe₄₉Rh₅₁, *Phys. Rev. B* 89 (2014) 214105.
- [8] J. Ganping, J. Hohlfeld, B. Bergman, R.J.M. van de Veerdonk, O.N. Mryasov, J.-Y. Kim, G. Ju, X. Wu, D. Weller, B. Koopmans, Ultrafast generation of ferromagnetic order via a laser-induced phase transformation in FeRh thin films, *Phys. Rev. Lett.* 93 (2004) 197403.
- [9] F. Pressacco, V. Uhlir, M. Gatti, A. Bendounan, E.E. Fullerton, F. Sirotti, Stable room-temperature ferromagnetic phase at the FeRh(100) surface, *Sci. Rep.* 6 (2016) 22383.
- [10] R. Fan, C.J. Kinane, T.R. Charlton, R. Dorner, M. Ali, M.A. De Vries, R.M.D. Brydson, C.H. Marrows, B.J. Hickey, D.A. Arena, B.K. Tanner, G. Nisbet, S. Langridge, Ferromagnetism at the interfaces of antiferromagnetic FeRh epilayers,

- Phys. Rev. B 82 (2010) 184418.
- [11] D. Odkhuu, Interfacial magnetic-phase transition mediated large perpendicular magnetic anisotropy in FeRh/MgO by a heavy transition-metal capping, *Sci. Rep.* 8 (2018) 6900.
- [12] D. Odkhuu, Magnetization reversal of giant perpendicular magnetic anisotropy at the magnetic-phase transition in FeRh films on MgO, *Phys. Rev. B* 93 (2016) 64412.
- [13] C. Bordel, J. Juraszek, D.W. Cooke, C. Baldasseroni, S. Mankovsky, J. Minar, Fe Spin reorientation across the metamagnetic transition in strained FeRh thin films, *Phys. Rev. Lett.* 109 (2012) 117201.
- [14] H. Kumar, D.R. Cornejo, S.L. Morelhaio, S. Kycia, I.M. Montellano, N.R. Alvarez, G. Alejanro, A. Butera, Strain effects on the magnetic order of epitaxial FeRh thin films, *J. Appl. Phys.* 124 (2018) 85306.
- [15] G. Zheng, S. Ke, M. Miao, J. Kim, R. Ramesh, N. Kioussis, Epitaxial strain controlled magnetocrystalline anisotropy in ultrathin FeRh/MgO bilayers, *AIP Adv.* 7 (2017) 55914.
- [16] D. Odkhuu, Role of the interfacial Rh-layer on robust ferromagnetism and large perpendicular magnetic anisotropy of FeRh films on MgO(0 0 1), *J. Magn. Magn. Mater.* 476 (2019) 487.
- [17] S. Jekal, S.H. Rhim, S.C. Hong, W.J. Son, A.B. Shick, Surface-termination-dependent magnetism and strong perpendicular magnetocrystalline anisotropy of an FeRh (0 0 1) thin film, *Phys. Rev. B* 92 (2015) 64410.
- [18] G. Zheng, S. Ke, M. Miao, J. Kim, R. Ramesh, N. Kioussis, Electric field control of magnetization direction across the antiferromagnetic to ferromagnetic transition, *Sci. Rep.* 7 (2017) 5366.
- [19] J. Kim, R. Ramesh, N. Kioussis, Revealing the hidden structural phases of FeRh, *Phys. Rev. B* 94 (2016) 180407(R).
- [20] M. Castiella, C. Gatel, J.F. Bobo, R. Tan, M. Respaud, M.J. Casanove, Structural investigation of magnetic FeRh epitaxial films, *Mater. Res. Express* 2 (2015) 86401.
- [21] N. Spiridis, J. Korecki, Influence of Au reconstruction on growth of Fe on Au(1 0 0), *Appl. Surf. Sci.* 141 (1999) 313.
- [22] S. Inoue, H.Y.Y. Ko, T. Suzuki, Magnetic properties of single-crystalline FeRh alloy thin films, *IEEE Trans. Magn.* 44 (2008) 2875.
- [23] P. Drózdź, M. Ślęzak, K. Matlak, B. Matlak, K. Freindl, D. Wilgocka-Ślęzak, N. Spiridis, J. Korecki, T. Ślęzak, Switching of Co magnetization driven by anti-ferromagnetic-ferromagnetic phase transition of FeRh alloy in Co/FeRh bilayers, *Phys. Rev. Appl.* 9 (2018) 034030.
- [24] P. Drózdź, M. Ślęzak, K. Matlak, D.W. Ślęzak, J. Korecki, T. Ślęzak, K. Matlak, Temperature controlled Fe/Au/FeRh spin valves, *AIP Adv.* 8 (2018) 101434.
- [25] G.C. Han, J.J. Qiu, Q.J. Yap, P. Luo, D.E. Laughlin, J.G. Zhu, T. Kanbe, T. Shige, Magnetic stability of ultrathin FeRh films, *J. Appl. Phys.* 113 (2013) 17C107.
- [26] K. Lagarec, Recoil 1.05 Mössbauer Analysis Software for Windows, © 1998, (2002).
- [27] G. Shirane, C.W. Chen, P.A. Flinn, R. Nathans, Hyperfine fields and magnetic moments in the Fe-Rh system, *J. Appl. Phys.* 34 (1963) 1044.
- [28] G. Shirane, C.W. Chen, P.A. Flinn, R. Nathans, Mossbauer study of hyperfine fields and isomer shifts in the Fe-Rh alloys, *Phys. Rev.* 131 (1963) 183.
- [29] J. van Driel, R. Coehoorn, G.J. Strijkers, E. Bruck, F.R. Boer, Compositional dependence of the giant magnetoresistance in thin films FeRh, *J. Appl. Phys.* 85 (1999) 1026.
- [30] E. Młyńczak, K. Freindl, N. Spiridis, J. Korecki, Epitaxial MgO/Fe(0 0 1) and Fe/MgO(0 0 1): structures of the interfaces, *J. Appl. Phys.* 113 (2013) 24320.